

pubs.acs.org/JACS Article

Charging a Negatively Curved Nanographene and Its Covalent Network

Yiqun Zhang,[#] Yikun Zhu,[#] Danni Lan,[#] Sai Ho Pun, Zheng Zhou, Zheng Wei, Ying Wang, Hung Kay Lee, Chao Lin, Jiangpeng Wang, Marina A. Petrukhina,* Quan Li,* and Qian Miao*



Cite This: J. Am. Chem. Soc. 2021, 143, 5231-5238



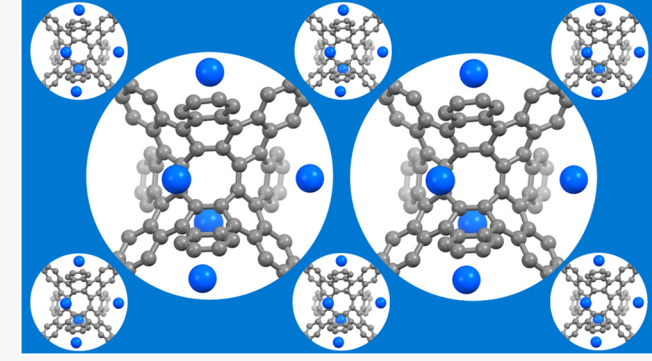
ACCESS

III Metrics & More



s Supporting Information

ABSTRACT: This study explores a bottom-up approach toward negatively curved carbon allotropes from octabenzo[8]circulene, a negatively curved nanographene. Stepwise chemical reduction reactions of octabenzo[8]circulene with alkali metals lead to a unique highly reduced hydrocarbon pentaanion, which is revealed by X-ray crystallography suggesting a local view for the reduction and alkali metal intercalation processes of negatively curved carbon allotropes. Polymerization of the tetrabromo derivative of octabenzo[8]circulene by the nickel-mediated Yamamoto coupling reaction results in a new type of porous carbon-rich material, which consists of a covalent network of negatively curved nanographenes. It has a specific surface area of 732 m² g⁻¹ and functions as anode material for lithium ion batteries exhibiting a maximum capacity of



830 mAh·g⁻¹ at a current density of 100 mA·g⁻¹. These results indicate that this covalent network presents the key structural and functional features of negatively curved carbon allotropes.

■ INTRODUCTION

Carbon allotropes comprised exclusively of sp²-hybridized carbon atoms have fascinated the scientific community with their esthetic nanostructures and unparalleled physical properties over the last several decades. Such allotropes including fullerenes, carbon nanotubes, and graphene present flat or curved surfaces whose overall geometric feature is reflected by a geometric quantity called the polygonal curvature of the surface.² Consisting of six-membered rings exclusively, graphene has zero curvature. Five-membered rings induce positive curvature as displayed in fullerenes, while seven-membered, eight-membered, or larger rings in a hexagonal lattice of carbon induce negative curvature as displayed in a saddle-shaped surface. Negatively curved threedimensional periodic covalent networks of sp² carbon atoms are known as Mackay crystals or carbon schwarzites, which are named after A. L. Mackay and H. A. Schwarz, respectively. Mackay, together with Terrones, first proposed negatively curved carbon allotropes³ by embedding octagons in the graphitic lattice in 1991, while Schwarz in the 1880s first described the triply periodic minimal surface, the topological model for Mackay crystals.4 Carbon schwarzites are a longsought-after target in carbon nanoscience but have not been synthesized unambiguously yet. 5,6 Interesting properties and potential applications of carbon schwarzites are predicted on the basis of computational studies.^{7,8} First-principles calculations suggest potential application of carbon schwarzites in lithium ion batteries as new anode materials,⁹ where the negatively curved surface binds lithium ions with higher affinity than a flat surface¹⁰ and the presence of pores enable three-dimensional lithium ion diffusion paths with relatively small energy barriers. Fragments that contain key structural information on carbon schwarzites are negatively curved nanographenes,^{11–16} which have polycyclic aromatic frameworks containing seven-,^{17–27} eight-membered^{28–35} or larger rings. They are proposed as templates or monomers in synthesis of carbon schwarzites in a bottom-up approach.^{15,16,32}

As inspired by the concept of bottom-up approach, we envisioned that linking negatively curved nanographenes into a network through C—C single bonds results in a new type of carbon-rich material, which can mimic negatively curved carbon allotropes with respect to both structure and function. When the covalent network functions as the anode material in lithium ion batteries, its negatively curved polycyclic aromatic units are reduced during the charging process and interact with lithium ions. Therefore, studying chemical reduction of

Received: February 10, 2021 Published: March 25, 2021





negatively curved nanographenes by alkali metals can provide a local view for the reduction and metal intercalation processes in the anode materials in lithium ion batteries, shedding light on the structure—property relationship for advancement of the anode materials on the basis of negatively curved nanocarbons. One of the scientific motivations that drove this study is to reveal whether negatively curved polycyclic arenes are similar to positively curved carbon π -bowls in acquiring multiple electrons in stepwise chemical reduction reactions with alkali metals³⁶ or exhibit unique metal intercalation patterns. ^{37,38} The negatively curved nanographene explored herein is octabenzo[8]circulene (**OB8C**)³² as shown in Figure 1.

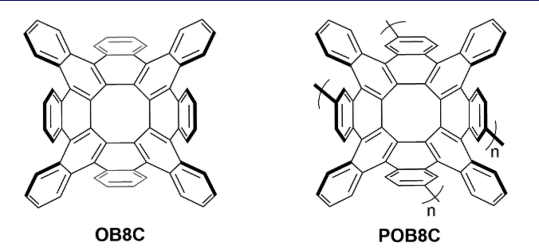


Figure 1. Structures of octabenzo[8]circulene (OB8C) and its covalent network POB8C.

Detailed below are the chemical reduction of OB8C with alkali metals, synthesis of the covalent network of OB8C (POB8C in Figure 1) by polymerization of a tetrabromo derivative of OB8C, and the performance of POB8C as anode material for lithium ion batteries.

■ RESULTS AND DISCUSSION

Chemical and Electrochemical Reduction of OB8C. The chemical reduction of OB8C with Li and Na metals in THF was investigated at room temperature and monitored with in situ UV-vis spectroscopy. Multiple reduction steps accompanied by notable color changes were detected for these reactions as detailed in the Supporting Information. The Nainduced reaction quickly progressed through the formation of intermediate brown, purple, and green solutions until it reached the final brown-purple color (λ_{max} = 475 nm, Figure S1) with prolonged reaction time. It is worth noting that these multiple reduction steps proceed very fast (over ca. 45 min), thus thwarting our attempts to isolate the transient reduction intermediates. An excess of Na metal with prolonged reaction time was finally used to ensure the formation of the highest reduction stage of OB8C. Slow diffusion of hexanes to the reaction solution in THF at this stage led to isolation of a highly reduced product as a crystalline material after 5 days. Single-crystal X-ray diffraction analysis revealed its composition to be [Na⁺(18-crown-6)(THF)₂]₂[Na⁺(18-crown-6)-(THF)][$\{Na^{+}_{2}(THF)_{3}\}(OB8C^{5-})$] $\cdot 4.5THF$. Notably, the reaction of OB8C with Li metal followed the same steps as that with Na but, after extended reaction time, led to a solution of a distinctive violet color (Figure S2). This violet solution may be attributed to formation of a higher reduced state than the pentareduced anion or be explained by the sensitivity of the absorption spectra of anionic π -systems to their coordination environments.

Figure 2a shows the crystal structure of the sodium salt of the OB8C pentaanion, which includes five crystallographically independent Na⁺ ions. Two sodium ions (Na1 and Na2) occupy structural pockets formed by the negatively curved core

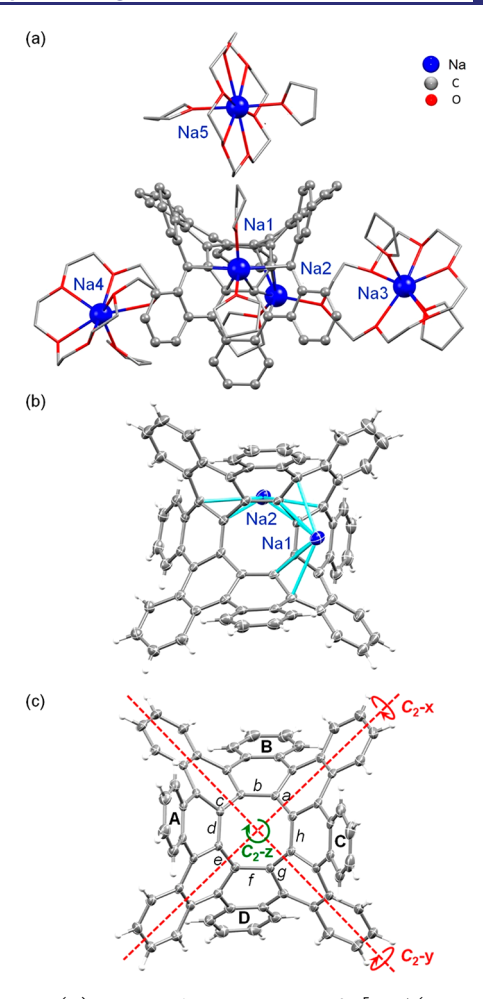


Figure 2. (a) Crystal structure of $[Na^+(18\text{-crown-6})(THF)_2]_2[Na^+(18\text{-crown-6})(THF)][\{Na^+_2(THF)_3\}(OB8C^5^-)];$ (b) $[Na^+_2(OB8C^5^-)]^{3-}$ in the crystal; (c) OB8C in the crystal structure of OB8C·2THF. (In panel a, H atoms are removed for clarity, Na atoms and C atoms in OB8C are shown as balls, and other atoms are shown as sticks. In panels b and c, Na and C atoms are shown as ellipsoids at 50% probability level.)

of OB8C⁵⁻, while the other three sodium ions (Na3, Na4, and Na5) remain solvent-separated from the OB8C⁵⁻ anion. Specifically, Na1 binds to the internal surface of OB8C⁵⁻ with Na-C distances ranging over 2.616(5)-2.855(5) Å and is also capped by two THF molecules (Na-O_{THF}: 2.190(20)/ 2.224(4) Å) (Figure S10). Na2 binds to the opposite side of the pentaanion core (Na-C: 2.560(5)-3.003(5) Å) and has one coordinated THF molecule (Na-O_{THF}: 2.120(30) Å). Two external sodium ions (Na3 and Na5) are wrapped by one 18-crown-6 (Na-O_{crown}: 2.420(20)-2.535(18) Å and 2.500(6)-2.967(7) Å, respectively) and two THF molecules $(Na-O_{THF}: 2.338(7)/2.427(9) \text{ Å and } 2.312(15)/2.359(13)$ Å). In contrast, Na4 is coordinated by one THF molecule (Na-O_{THE}: 2.303(7) Å) and one highly twisted 18-crown-6 ligand (Na-O_{crown}: 2.425(7)-2.561(6) Å). In addition, Na2 also exhibits a short contact (2.293(16) Å) with one O atom of the 18-crown-6 ligand bound to Na3. All Na···C and Na···O distances are comparable to those previously reported. $^{39-41}$

For direct structural comparison of the neutral and pentareduced states of **OB8C**, crystals of neutral **OB8C** were also isolated (see the Supporting Information for more details) and characterized by X-ray diffraction as **OB8C**·2THF (Figure

S9). In the neutral state, the OB8C molecule is more twisted, as mainly observed on the peripheral phenyl rings. Parts b and c of Figure 2 compare the structures of $[\{Na^{+}_{2}(OB8C^{5-})\}]^{3-}$ and neutral OB8C in the crystals. OB8C is shaped like a twisted saddle with approximate D_2 symmetry, which deviates from the D_{2d} symmetry predicted by the density functional theory (DFT) calculations. Figure 2c shows the three C_2 symmetry axes of OB8C, C_2 -x, C_2 -y, and C_2 -z, which are perpendicular to each other. In comparison to the neutral form, the pentaanion is less twisted and closer to the D_{2d} symmetry. Comparisons of the dihedral and torsion angles and bond lengths in OB8C⁵⁻ and OB8C are detailed in Tables S2 and S3. Briefly, the dihedral angles between the rings A and C and the rings B and D of 11.4° and −11.1° in neural OB8C, respectively, are dramatically reduced to 1.2° and -2.3° in OB8C⁵⁻ (Figure S12). Accordingly, the central eightmembered ring becomes more symmetric upon electron charging with torsion angles b-f and d-h measured at -0.2° and 2.8° in OB8C⁵⁻ in comparison to those of -11.4° and 10.4° observed in the more distorted neutral state. This is accompanied by significant bond length changes in the central eight-membered ring in OB8C⁵⁻ vs those in OB8C (Scheme in Table S2). Specifically, the C-C bond lengths at positions b, d, f, and h ranging over 1.460(3)-1.472(3) Å in **OB8C** are shortened by about 0.08 Å in OB8C5- (1.379(7)-1.398(7) Å). In contrast, the bonds at a, c, e, and g (1.445(3)-1.463(3))Å in OB8C) are slightly elongated upon five-electron addition (1.464(6)-1.486(7) Å). In $[\text{Na}_{2}^{+}(\text{OB8C}^{5-})]^{3-}$, the Na⁺ ions occupy the spaces above and below the saddle of OB8C, and each Na+ coordinates four carbon atoms in the eightmembered ring and two adjacent carbon atoms. This is in agreement with the electrostatic potential map of OB8C5-(Figure 3), which shows high negative charge in the central

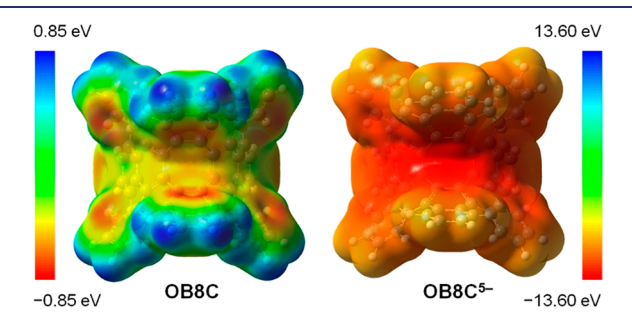


Figure 3. Electrostatic potential maps on the 0.002 isodensity surface of neutral **OB8C** (left) and **OB8C**⁵⁻ (right) pentaanion calculated at the B3LYP level of DFT with 6-31G(d,p) basis set.

valley. In contrast, the electrostatic potential map of neutral OB8C shows the most negative electrostatic potential at the center of peripheral benzene rings.

In the solid state, molecules of **OB8C** self-assemble into a layered structure and the space between layers of **OB8C** are occupied by the cocrystallized solvent (THF) molecules. As a result of its approximate D_2 symmetry, OB8C is chiral and exists as a pair of enantiomers in the crystals. Figure 4a shows one layer of **OB8C** in the bc plane, where two enantiomers are colored in light green and light blue, respectively. In this layer, one molecule of **OB8C** interlocks with two adjacent enantiomers by inserting one periphery benzene ring into the space below the saddle of one adjacent enantiomer. Such interlocking is not available in the reduced form of **OB8C**

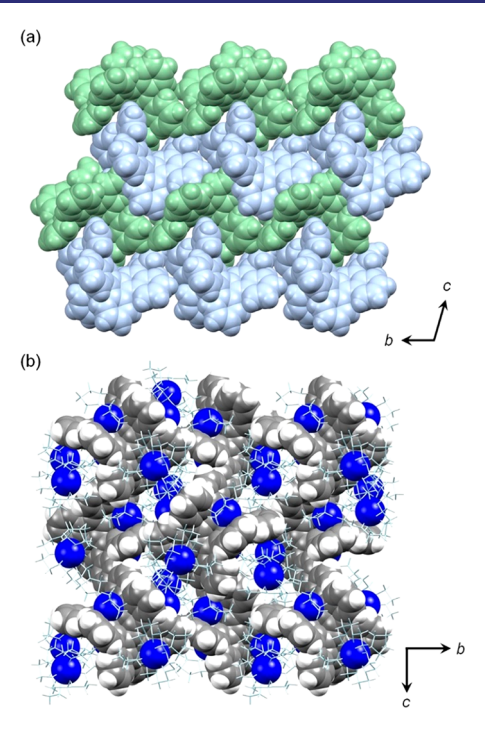


Figure 4. Solid-state packing of (a) OB8C (two enantiomers are shown in light green and light blue space-filling models, respectively), and (b) $[\mathrm{Na}^+(18\text{-crown-6})(\mathrm{THF})_2]_2[\mathrm{Na}^+(18\text{-crown-6})(\mathrm{THF})]_{\{\mathrm{Na}^+_2(\mathrm{THF})_3\}(\mathrm{OB8C}^{5-})\}}$ (mixed model; 18-crown-6 ether and coordinated THF molecules are shown in light blue). Interstitial THF molecules are not shown.

because the space above and below the saddle is occupied by Na⁺ cations. Instead, a three-dimensional network (Figure 4b) is formed through multiple $C-H\cdots\pi$ interactions between the highly negatively charged pentaanions of **OB8C** and the {Na⁺(18-crown-6)(THF)_n} (n=1 and 2) cationic moieties, with contacts ranging from 2.503(8) Å to 2.743(8) Å. The contorted and twisted core of **OB8C** (see Table S2 for dihedral and torsion angles) allows for the formation of internal cavities that are filled by interstitial THF molecules in both crystal structures without any notable interactions.

The electron paramagnetic resonance (EPR) spectrum collected from the crystals that were sealed in a glass capillary under argon exhibited a signal typical for organic radicals (Figure S5). The lack of fine structures suggests the spin is localized inside the π -backbone of **OB8C** without coupling with the peripheral hydrogen atoms. This is also in agreement with the observed high negative charge in the central valley of **OB8C**⁵⁻ in its electrostatic potential map (Figure 3). Consistent with the radical nature of **OB8C**⁵⁻ based on the EPR, the ¹H NMR spectrum of the crystals dissolved in THF- d_8 was silent in the aromatic region and showed only signals of 18-crown-6 and THF (Figure S6).

The electrochemical reduction of **OB8C** was studied with cyclic voltammetry (CV) under different conditions. When **OB8C** was dissolved in a mixed solvent of o-dichlorobenzene/ acetonitrile (4:1), the cyclic voltammogram with a scan rate of 25 mVs⁻¹ exhibited two pseudoreversible single-electron reduction waves with half-wave potentials of -1.88 and -2.00 V versus ferrocenium/ferrocene (Fc⁺/Fc) as shown in Figure 5. Avoiding o-dichlorobenzene as the solvent can allow a wider test window of CV. However, **OB8C** is not soluble in acetonitrile, and the CV of **OB8C** collected from the solution

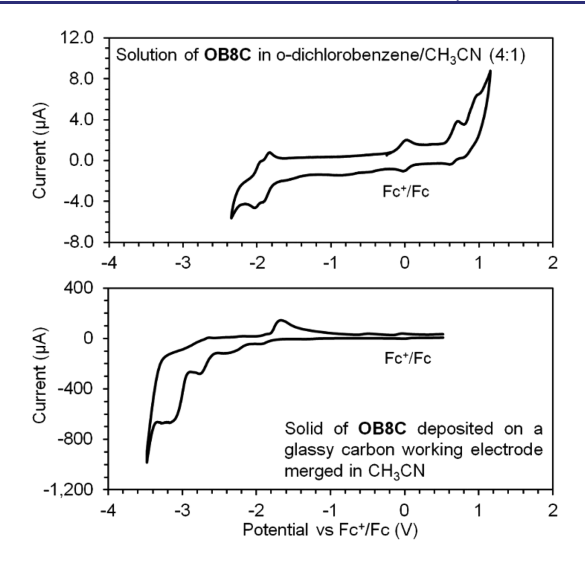


Figure 5. Cyclic voltammograms of **OB8C** measured from a solution in o-dichlorobenzene/acetonitrile (4:1) containing 0.1 M of tetrabutylammonium hexafluorophosphate as the supporting electrolyte with a scan rate of 25 mVs $^{-1}$ (top) and a film deposited a glassy carbon working electrode immerged in CH $_3$ CN with a scan rate of 50 mVs $^{-1}$ (bottom).

in THF (Figure S8) shows weak and poorly resolved reduction peaks presumably due to its low solubility in THF, although THF was used as the solvent for chemical reduction of **OB8C** with alkali metals. Therefore, **OB8C** was drop-cast onto a glassy carbon electrode for further electrochemical measurement in acetonitrile at a scan rate of 50 mVs $^{-1}$. Four irreversible reduction peaks were observed at -1.91, -2.26, -2.76, and -3.18 V versus Fc^+/Fc , and another reduction peak was barely observable at -3.28 V versus Fc^+/Fc (Figure 5). The obseration of multiple reduction waves in the cyclic voltammograms is in agreement with the multiple electron chemical reduction of **OB8C** by alkali metals.

Covalent Networks. In order to link OB8C molecules into a covalent network, tetrabromooctabenzo [8] circulene (1) was synthesized by modifying the reported synthesis of OB8C³² and then polymerized through nickel-mediated Yamamoto coupling reaction as shown in Scheme 1. Treatment of tetrabromide 2 with potassium tert-butoxide enabled elimination of HBr from 2 giving diyne 3, which was not purified or characterized due to its poor solubility. The subsequent 2-fold Diels-Alder reactions of 3 with 1,3-bis(4bromophenyl)isobenzofuran (4)⁴² gave the adduct 5 as a mixture of diastereomers in a yield of 53%. Reaction of 5 with iodotrimethylsilane and sodium iodide afforded 6 with the oxygen bridges cleaved. The Scholl reaction of 6 with 2,3dichloro-5,6-dicyano-1,4-benzoquinone (DDQ) in triflic acid resulted in 1 in a yield of 56%. Finally, polymerization of 1 was carried out in dry DMF through nickel-mediated Yamamoto homocoupling reaction⁴³ resulting in the covalent network POB8C in a good yield (82%). The resulting POB8C is a red powder, which is insoluble in common organic solvents.

The red powders of **POB8C** were characterized with different techniques. The elemental analysis reveals 91.40% of C, 3.92% of H, and 1.39% of Br. The molar ratio of Br to C is 0.00229, indicating that, on average, each unit of **OB8C** in the polymer has 0.146 atom of Br unreacted. The low ratio of unreacted Br suggests formation of a covalent network rather than oligomers because even if one C-Br bond in each

Scheme 1. Synthesis of Covalent Network POB8C

molecule of 1 remained intact during the coupling reaction, formation of three C-C single bonds to each repeating unit would guarantee a network. In comparison to POB8C, the reported two-dimensional conjugated aromatic polymer that was synthesized from tetrabromopolyaromatic monomers via C-C coupling reactions has 0.213 atom of Br unreacted per repeating unit.⁴⁴ The rest of the mass (3.29%) can be attributed to oxygen as a result of oxidation of the OB8C units by O₂ in air. This is in agreement with the fact that the mass spectrum from the crystalline powders of **OB8C** $(C_{64}H_{32})$ stored in air at room temperature for six months exhibited molecular ion peaks with m/z of 816.2456 and 832.2387, which correspond to oxidation products, C₆₄H₃₂O and C₆₄H₃₂O₂, respectively. The oxidation of **POB8C**, particularly on the surface, is further supported by its X-ray photoelectron spectrum (XPS), which exhibits a major peak at 285.0 eV and a minor peak at 533.4 eV corresponding to C (sp²) and O atoms, respectively (Figure S19). The observed oxidation of POB8C is similar to that of a recently reported threedimensional sp-sp³ hybridized porous carbon material.⁴⁵

The X-ray diffraction from the powders of **POB8C** (Figure S20) exhibits two broad peaks centered at about $2\theta = 7^{\circ}$ and 22° , indicating existence of short-range order but lack of longrange order in this material. The peak at $2\theta = 7^{\circ}$ corresponds to a *d*-spacing of 1.3 nm, which is roughly in agreement with the size of OB8C unit (1.46 nm). The thermogravimetric analysis (TGA) indicates that **POB8C** is thermally stable with only 2.2% and 3.2% loss of weight when heated to 200 and 300 °C, respectively. The IR spectrum of **POB8C** (Figure S19) is very similar to that of **OB8C** exhibiting absorption peaks

attributable to the stretching and bending of C-H bonds and the stretching of C-C bonds. As shown in Figure S23a, the Raman spectrum of POB8C exhibits four major peaks at 1295, 1355, 1563, and 1606 cm⁻¹, which are in the D and G regions for graphitic materials, ^{24,46,47} respectively. In contrast, the Raman spectrum of OB8C (Figure S23b) exhibits two major peaks at 1293 and 1353 cm⁻¹ and a few minor peaks including those at 1566 and 1606 cm⁻¹, in agreement with the vibrational Raman spectrum of OB8C (Figure S23b) calculated at the B3LYP level of density functional theory (DFT) with the 6-311G(d,p) basis set. The calculated vibrational motions (Figure S24) indicate that the major peaks of OB8C at 1293 and 1353 cm⁻¹ can be attributed to the collective breathing motions⁴⁶ of the central [8]circulene moiety, while the minor peaks of OB8C at 1566 and 1606 cm⁻¹ can be attributed to the stretching and waggling motions⁴⁷ of the peripheral benzene rings. In POB8C, the collective breathing motions of the central [8] circulene in each unit are almost unchanged giving rise to the peaks of POB8C at 1295 and 1355 cm⁻¹, while the stretching and waggling motions of the peripheral benzene rings are largely affected by the formation of C-C single bonds between the OB8C units giving rise to the enhanced peaks of POB8C at 1563 and 1606 cm⁻¹. The transmission electron microscopy (TEM) image (Figure S25) taken from POB8C also suggests formation of porous networks. The porosity of POB8C was characterized with nitrogen adsorption measurements at 77 K, which show a specific surface area of 732 m² g⁻¹. This value surpasses that of multiwalled carbon nanotubes (204 m² g⁻¹)⁴⁸ and graphdiyne $(321 \text{ m}^2 \text{ g}^{-1})^{49}$ and is comparable to that of the threedimensional sp-sp³-hybridized porous carbon material (766 m² g⁻¹).⁴⁵ The pore size distribution (Figure S26) derived from the nitrogen uptake isotherm at 77 K shows a peak centered at 3.78 nm.

To evaluate the performance of POB8C as the anode material for lithium ion batteries, coin cells were assembled using Li foil as the counter electrode⁵⁰ as detailed in the Supporting Information, and their discharge/charge behaviors and electrochemical properties were studied. Figure 6a shows the first three cycle discharge/charge profiles of the POB8C electrode at a current density of 100 mA·g⁻¹. The initial discharge/charge cycle involves a large irreversible capacity and a low initial Coulombic efficiency (20%). After the initial cycle, it delivers a discharge capacity of 670 mAh·g⁻¹ in the second discharging and a reversible capacity of 459 mAh·g⁻¹ in the second charging. This discharge capacity is higher than that of graphite (372 mAh·g⁻¹, based on the fundamental Li ion storage limit of LiC₆)⁹ by 80%, in agreement with its porous structure. When the discharge/charge process was cycled 200 times, the discharge capacity exhibited a slow activation reaching a maximum of 830 mAh·g⁻¹ after 66 cycles and then gradually dropped to 546 mAh·g⁻¹ in the 200th cycle, and the Coulombic efficiency increased to higher than 98% after 20 cycles as shown in Figure 6b. The maximum discharge capacity of POB8C is comparable to that of disordered graphene nanosheets $(794-1054 \text{ mAh g}^{-1})^{51}$ and those of many composite materials based on three-dimensional porous graphene networks⁵² but lower than that of curled graphene nanosheets (1264 mA h g⁻¹).⁵³ As shown in Figure 6c, the cyclic voltammogram (CV) of the **POB8C** in the first cycle exhibits cathodic peaks centered at 0.35, 0.89, and 1.40 V versus Li⁺/Li, which are not observed in the second to fifth cycles. These peaks can be attributed to two processes. First,

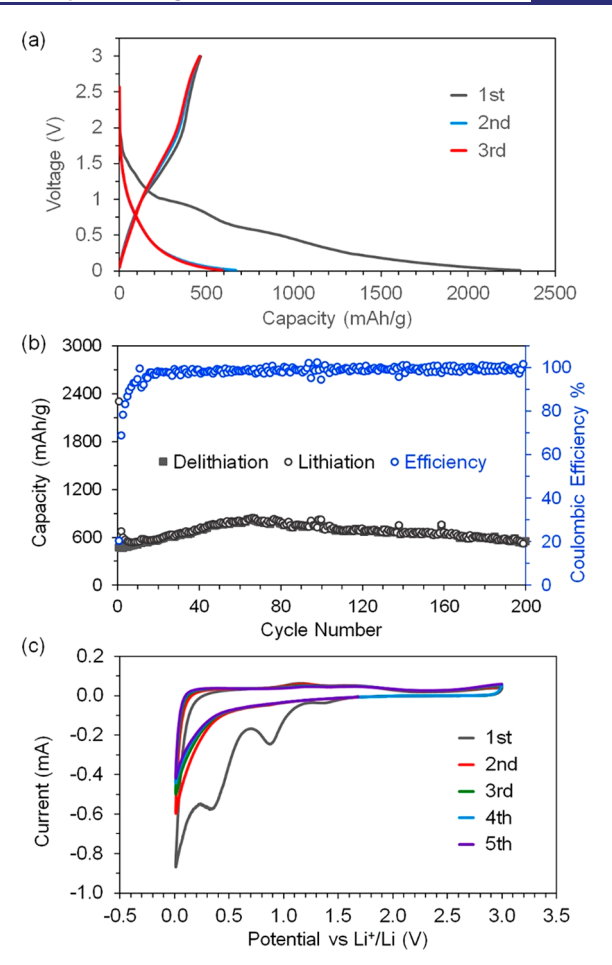


Figure 6. (a) First three discharge–charge profiles of **POB8C** at a current density of 100 mA·g $^{-1}$; (b) cycling performance of **POB8C** at a current density of 100 mA·g $^{-1}$ showing the charge capacity (solid square) and discharge capacity (black circle) and Coulombic efficiency (blue circle); (c) cyclic voltammograms of the first five cycles for **POB8C** at a scan rate of 0.1 mV s $^{-1}$ in an electrochemical window of 0.01–3.0 V.

formation of a solid electrolyte interphase (SEI) layer⁵⁴ on the electrode surface is a common reason for irreversible capacity. Second, the peaks at 0.35 and 0.89 V versus Li⁺/Li correspond to -3.33 V and -2.79 V versus Fc^+/Fc (calculated on the basis of the standard reduction potentials of Li⁺/Li and Fc⁺/Fc, which are -3.04 V versus NHE⁵⁵ and 0.64 V versus NHE,⁵⁶ respectively). They are very close to the reduction potentials of **OB8C** at -3.28 V and -2.76 V versus Fc^+/Fc (Figure 5), and thus may be attributed to the reduction of the OB8C repeating units in the covalent networks. The irreversible nature of these peaks suggests that these reduction processes are associated with strong interactions of Li⁺ cations with OB8C, possibly at the central valley as suggested by the crystal structure of OB8C⁵⁻. The CV of POB8C also exhibits a large cathodic peak close to 0.0 V, which becomes weaker after the first cycle. This peak is typical for graphite⁵⁷ and different forms of graphene, 58,59 to which intercalation of lithium ions is in accompany with a potential very close to that of metallic lithium. The above observations from CV are in agreement with the large irreversible capacity in the initial discharging and a low initial Coulombic efficiency.

CONCLUSIONS

In conclusion, the above study puts forth a bottom-up approach toward negatively curved carbon allotropes by covalently linking negatively curved nanographenes (OB8C) into a network. In connection with the application of this covalent network as anode material for lithium ion batteries, OB8C was found able to acquire multiple electrons in stepwise reduction reactions with two alkali metals (Li and Na) in solution, as revealed spectroscopically. Importantly, the highly reduced pentaanion of OB8C has been crystallized with five sodium counterions to exhibit unique metal intercalation patterns as revealed by X-ray crystallography. Polymerization of the tetrabromo derivative of OB8C by a nickel-mediated Yamamoto coupling reaction resulted in POB8C, which is a new type of porous carbon-rich material having a specific surface area of 732 m² g⁻¹. It functioned as the anode material for lithium ion batteries exhibiting a maximum discharge capacity of 830 mAh·g⁻¹ at a current density of 100 mA·g⁻¹ These results indicate that POB8C presents the key structural and functional features of negatively curved carbon allotropes. However, because POB8C lacks long-range order, it still cannot mimic carbon schwarzites in the aspect of periodical structures. We envision long-range order can be achieved by constructing covalent organic frameworks (COFs) of negatively curved nanographenes through formation of dynamic covalent bonds, 60 as inspired by the recent success in synthesis of COFs of fullerene and corannulene. 61,62 Research in this direction is in progress in our laboratory.

ASSOCIATED CONTENT

Supporting Information

The Supporting Information is available free of charge at https://pubs.acs.org/doi/10.1021/jacs.1c01642.

Details of reduction of **OB8C** with alkali metals, crystal structure solution and refinement, synthesis and characterization, fabrication and characterization of coin cells (PDF)

Accession Codes

CCDC 2043131–2043132 contain the supplementary crystallographic data for this paper. These data can be obtained free of charge via www.ccdc.cam.ac.uk/data_request/cif, or by emailing data_request@ccdc.cam.ac.uk, or by contacting The Cambridge Crystallographic Data Centre, 12 Union Road, Cambridge CB2 1EZ, UK; fax: +44 1223 336033.

AUTHOR INFORMATION

Corresponding Authors

Marina A. Petrukhina — Department of Chemistry, University at Albany, State University of New York, Albany, New York 12222, United States of America; orcid.org/0000-0003-0221-7900; Email: mpetrukhina@albany.edu

Quan Li — Department of Physics, The Chinese University of Hong Kong, Hong Kong, China; oorcid.org/0000-0001-8563-1802; Email: liquan@phy.cuhk.edu.hk

Qian Miao – Department of Chemistry, The Chinese University of Hong Kong, Hong Kong, China; orcid.org/ 0000-0001-9933-6548; Email: miaoqian@cuhk.edu.hk

Authors

Yiqun Zhang — Department of Chemistry, The Chinese University of Hong Kong, Hong Kong, China; orcid.org/ 0000-0001-9520-701X

- Yikun Zhu Department of Chemistry, University at Albany, State University of New York, Albany, New York 12222, United States of America
- Danni Lan Department of Physics, The Chinese University of Hong Kong, Hong Kong, China
- Sai Ho Pun Department of Chemistry, The Chinese University of Hong Kong, Hong Kong, China
- **Zheng Zhou** Department of Chemistry, University at Albany, State University of New York, Albany, New York 12222, United States of America
- Zheng Wei Department of Chemistry, University at Albany, State University of New York, Albany, New York 12222, United States of America
- Ying Wang Department of Chemistry, The Chinese University of Hong Kong, Hong Kong, China; orcid.org/ 0000-0002-6240-5535
- Hung Kay Lee Department of Chemistry, The Chinese University of Hong Kong, Hong Kong, China; orcid.org/0000-0002-2052-4069
- Chao Lin Department of Physics, The Chinese University of Hong Kong, Hong Kong, China
- Jiangpeng Wang Department of Physics, The Chinese University of Hong Kong, Hong Kong, China

Complete contact information is available at: https://pubs.acs.org/10.1021/jacs.1c01642

Author Contributions

[#]Yiqun Zhang, Yikun Zhu, and Danni Lan contributed equally to this work.

Notes

The authors declare no competing financial interest.

ACKNOWLEDGMENTS

Financial support for this work from the Research Grants Council of Hong Kong (GRF 14300919) is gratefully acknowledged by Q.M., and financial support from the U.S. National Science Foundation (CHE-2003411) is gratefully acknowledged by M.A.P. NSF's ChemMatCARS Sector 15 is principally supported by the Divisions of Chemistry (CHE) and Materials Research (DMR), National Science Foundation, under Grant No. NSF/CHE-1834750. The use of the Advanced Photon Source, an Office of Science User Facility operated for the U.S. Department of Energy (DOE) Office of Science by Argonne National Laboratory, was supported by the U.S. DOE under Contract No. DE-AC02-06CH11357.

■ REFERENCES

- (1) Rickhaus, M.; Mayor, M.; Juríček, M. Chirality in Curved Polyaromatic Systems. *Chem. Soc. Rev.* **2017**, *46*, 1643–1660.
- (2) Venema, G. A. Polygonal Models and the Geometry of Space. In Foundations of Geometry, 2nd ed.; Pearson: Boston, 2012; Chapter 12. (3) Mackay, A. L.; Terrones, H. Diamond from Graphite. Nature 1991, 352, 762.
- (4) Terrones, H. Fullerenes and Beyond: Complexity, Morphology, and Functionality in Closed Carbon Nanostructures. In *Springer Handbook of Nanomaterials*; Vajtai, R., Ed.; Springer: Berlin, 2013; Chapter 3.
- (5) Kim, K.; Lee, T.; Kwon, Y.; Seo, Y.; Song, J.; Park, J. K.; Lee, H.; Park, J. Y.; Ihee, H.; Cho, S. J.; Ryoo, R. Lanthanum-Catalysed Synthesis of Microporous 3D Graphene-like Carbons in a Zeolite Template. *Nature* **2016**, *535*, 131–135.
- (6) Braun, E.; Lee, Y.; Moosavi, S. M.; Barthel, S.; Mercado, R.; Baburin, I. A.; Proserpio, D. M.; Smit, B. Generating Carbon

- Schwarzites via Zeolite-Templating. Proc. Natl. Acad. Sci. U. S. A. 2018, 115, E8116.
- (7) Park, S.; Kittimanapun, K.; Ahn, J. S.; Kwon, Y. K.; Tomanek, D. Designing Rigid Carbon Foams. *J. Phys.: Condens. Matter* **2010**, 22, 334220.
- (8) Park, N.; Yoon, M.; Berber, S.; Ihm, J.; Osawa, E.; Tománek, D. Magnetism in All-Carbon Nanostructures with Negative Gaussian Curvature. *Phys. Rev. Lett.* **2003**, *91*, 237204.
- (9) Odkhuu, D.; Jung, D. H.; Lee, H.; Han, S. S.; Choi, S.-H.; Ruoff, R. S.; Park, N. Negatively Curved Carbon as the Anode for Lithium Ion Batteries. *Carbon* **2014**, *66*, 39–47.
- (10) Lu, Z. J.; Gao, D. L.; Yi, D.; Yang, Y. J.; Wang, X.; Yao, J. N. sp²/sp³ Hybridized Carbon as an Anode with Extra Li-Ion Storage Capacity: Construction and Origin. *ACS Cent. Sci.* **2020**, *6*, 1451–1459.
- (11) Narita, A.; Wang, X. Y.; Feng, X. L.; Müllen, K. New Advances in Nanographene Chemistry. Chem. Soc. Rev. 2015, 44, 6616–6643.
- (12) Segawa, Y.; Ito, H.; Itami, K. Structurally Uniform and Atomically Precise Carbon Nanostructures. *Nat. Rev. Mater.* **2016**, *1*, 15002.
- (13) Márquez, I. R.; Castro-Fernández, S.; Millán, A.; Campaña, A. G. Synthesis of Distorted Nanographenes Containing Seven- and Eight-Membered Carbocycles. *Chem. Commun.* **2018**, *54*, 6705–6718.
- (14) Majewski, M. A.; Stępień, M. Bowls, Hoops, and Saddles: Synthetic Approaches to Curved Aromatic Molecules. *Angew. Chem., Int. Ed.* **2019**, 58, 86–116.
- (15) Pun, S. H.; Miao, Q. Toward Negatively Curved Carbons. *Acc. Chem. Res.* **2018**, *51*, 1630–1642.
- (16) Miao, Q.; Yang, D. From Polycyclic Arenes Containing Eight-Membered Rings to Negatively Curved Nanocarbons: Progress and Outlook. *Prog. Chem.* **2020**, *32*, 1835–1845.
- (17) Luo, J.; Xu, X.; Mao, R.; Miao, Q. Curved Polycyclic Aromatic Molecules That Are π -Isoelectronic to Hexabenzocoronene. *J. Am. Chem. Soc.* **2012**, 134, 13796–13803.
- (18) Kawasumi, K.; Zhang, Q.; Segawa, Y.; Scott, L. T.; Itami, K. A Grossly Warped Nanographene and the Consequences of Multiple Odd-Membered-Ring Defects. *Nat. Chem.* **2013**, *5*, 739–744.
- (19) Cheung, K. Y.; Xu, X.; Miao, Q. Aromatic Saddles Containing Two Heptagons. J. Am. Chem. Soc. 2015, 137, 3910–3914.
- (20) Márquez, I. R.; Fuentes, N.; Cruz, C. M.; Puente-Munoz, V.; Sotorrios, L.; Marcos, M. L.; Choquesillo-Lazarte, D.; Biel, B.; Crovetto, L.; Gomez-Bengoa, E.; Gonzalez, M. T.; Martin, R.; Cuerva, J. M.; Campaña, A. G. Versatile Synthesis and Enlargement of Functionalized Distorted Heptagon-Containing Nanographenes. *Chem. Sci.* 2017, 8, 1068–1074.
- (21) Fukui, N.; Kim, T.; Kim, D.; Osuka, A. Porphyrin Arch-Tapes: Synthesis, Contorted Structures, and Full Conjugation. *J. Am. Chem. Soc.* **2017**, *139*, 9075–9088.
- (22) Gu, X.; Li, H.; Shan, B.; Liu, Z.; Miao, Q. Synthesis, Structure and Properties of Tetrabenzo[7]circulene. *Org. Lett.* **2017**, *19*, 2246–2249.
- (23) Oki, K.; Takase, M.; Mori, S.; Shiotari, A.; Sugimoto, Y.; Ohara, K.; Okujima, T.; Uno, H. Synthesis, Structures, and Properties of Core-Expanded Azacoronene Analogue: A Twisted Pi-System with Two N-Doped Heptagons. *J. Am. Chem. Soc.* **2018**, *140*, 10430–10434
- (24) Fernandez-Garcia, J. M.; Evans, P. J.; Rivero, S. M.; Fernandez, I.; Garcia-Fresnadillo, D.; Perles, J.; Casado, J.; Martin, N. π-Extended Corannulene-Based Nanographenes: Selective Formation of Negative Curvature. J. Am. Chem. Soc. 2018, 140, 17188–17196.
- (25) Pun, S. H.; Chan, C. K.; Luo, J.; Liu, Z.; Miao, Q. A Dipleiadiene-Embedded Aromatic Saddle Consisting of 86 Carbon Atoms. *Angew. Chem., Int. Ed.* **2018**, *57*, 1581–1586.
- (26) Farrell, J. M.; Grande, V.; Schmidt, D.; Wurthner, F. A Highly Warped Heptagon-Containing sp² Carbon Scaffold via Vinylnaphthyl π -Extension. *Angew. Chem., Int. Ed.* **2019**, *58*, 16504–16507.
- (27) Cheung, K. Y.; Miao, Q. A Ketone-Functionalized Aromatic Saddle as a Potential Building Block for Negatively Curved Carbon Nanobelts. *Chin. Chem. Lett.* **2019**, *30*, 1506–1508.

- (28) Sakamoto, Y.; Suzuki, T. Tetrabenzo[8]Circulene: Aromatic Saddles from Negatively Curved Graphene. J. Am. Chem. Soc. 2013, 135, 14074–14077.
- (29) Feng, C. N.; Kuo, M. Y.; Wu, Y. T. Synthesis, Structural Analysis, and Properties of [8] Circulenes. *Angew. Chem., Int. Ed.* **2013**, *52*, 7791–7794.
- (30) Miller, R. W.; Duncan, A. K.; Schneebeli, S. T.; Gray, D. L.; Whalley, A. C. Synthesis and Structural Data of Tetrabenzo[8] Circulene. *Chem. Eur. J.* **2014**, *20*, 3705–3711.
- (31) Cheung, K. Y.; Chan, C. K.; Liu, Z.; Miao, Q. A Twisted Nanographene Consisting of 96 Carbon Atoms. *Angew. Chem., Int. Ed.* **2017**, *56*, 9003–9007.
- (32) Pun, S. H.; Wang, Y.; Chu, M.; Chan, C. K.; Li, Y.; Liu, Z.; Miao, Q. Synthesis, Structures, and Properties of Heptabenzo-[7]Circulene and Octabenzo[8]Circulene. *J. Am. Chem. Soc.* **2019**, 141, 9680–9686.
- (33) Kirschbaum, T.; Rominger, F.; Mastalerz, M. A Chiral Polycyclic Aromatic Hydrocarbon Monkey Saddle. *Angew. Chem., Int. Ed.* **2020**, *59*, 270–274.
- (34) Pun, S. H.; Chan, C. K.; Liu, Z.; Miao, Q. An 80-Carbon Aromatic Saddle Enabled by a Naphthalene-Directed Scholl Reaction. *Org. Mater.* **2020**, *02*, 248–252.
- (35) Matsubara, S.; Koga, Y.; Segawa, Y.; Murakami, K.; Itami, K. Creation of Negatively Curved Polyaromatics Enabled by Annulative Coupling That Forms an Eight-Membered Ring. *Nat. Catal.* **2020**, *3*, 710–718.
- (36) Zabula, A. V.; Spisak, S. N.; Filatov, A. S.; Rogachev, A. Yu.; Petrukhina, M. A. Record Alkali Metal Intercalation by Highly Charged Corannulene. *Acc. Chem. Res.* **2018**, *51*, 1541–1549.
- (37) Spisak, S. N.; Rogachev, A. Yu.; Zabula, A. V.; Filatov, A. S.; Clerac, R.; Petrukhina, M. A. Tuning the Separation and Coupling of Corannulene Trianion-Radicals through Sizable Alkali Metal Belts. *Chem. Sci.* **2017**, *8*, 3137–3145.
- (38) Petrukhina, M. A. From Corannulene to Larger Carbon Bowls: Are They Better for Multiple Metal Encapsulation? *Dalton Trans.* **2019**, *48*, 5125–5130.
- (39) Spisak, S. N.; Wei, Z.; Rogachev, A. Yu.; Amaya, T.; Hirao, T.; Petrukhina, M. A. Double Concave Cesium Encapsulation by Two Charged Sumanenyl Bowls. *Angew. Chem., Int. Ed.* **2017**, *56*, 2582–2587
- (40) Zhou, Z.; Wang, X. Y.; Wei, Z.; Müllen, K.; Petrukhina, M. A. Charging OBO-Fused Double [5] Helicene with Electrons. *Angew. Chem., Int. Ed.* **2019**, *58*, 14969–14973.
- (41) Zhou, Z.; Wei, Z.; Tokimaru, Y.; Ito, S.; Nozaki, K.; Petrukhina, M. A. Stepwise Reduction of Azapentabenzocorannulene. *Angew. Chem., Int. Ed.* **2019**, *58*, 12107–12111.
- (42) Tozawa, H.; Kitamura, K.; Hamura, T. Water-Soluble 1,3-Diarylisobenzoheteroles: Syntheses and Characterization. *Chem. Lett.* **2017**, *46*, 703–706.
- (43) Yamamoto, T.; Morita, A.; Miyazaki, Y.; Maruyama, T.; Wakayama, H.; Zhou, Z. H.; Nakamura, Y.; Kanbara, T.; Sasaki, S.; Kubota, K. Preparation of π -Conjugated Poly(Thiophene-2,5-Diyl), Poly(p-Phenylene), and Related Polymers Using Zerovalent Nickel Complexes. Linear Structure and Properties of the π -Conjugated Polymers. *Macromolecules* **1992**, 25, 1214–1223.
- (44) Liu, W.; Luo, X.; Bao, Y.; Liu, Y. P.; Ning, G. H.; Abdelwahab, I.; Li, L.; Nai, C. T.; Hu, Z. G.; Zhao, D.; Liu, B.; Quek, S. Y.; Loh, K. P. A Two-Dimensional Conjugated Aromatic Polymer via C-C Coupling Reaction. *Nat. Chem.* **2017**, *9*, 563–570.
- (45) Zhao, Z.; Das, S.; Xing, G.; Fayon, P.; Heasman, P.; Jay, M.; Bailey, S.; Lambert, C.; Yamada, H.; Wakihara, T.; Trewin, A.; Ben, T.; Qiu, S.; Valtchev, V. A 3D Organically Synthesized Porous Carbon Material for Lithium-Ion Batteries. *Angew. Chem., Int. Ed.* **2018**, *57*, 11952–11956.
- (46) Maghsoumi, A.; Brambilla, L.; Castiglioni, C.; Müllen, K.; Tommasini, M. Overtone and combination features of G and D peaks in resonance Raman spectroscopy of the $C_{78}H_{26}$ polycyclic aromatic hydrocarbon. *J. Raman Spectrosc.* **2015**, *46*, 757–764.

- (47) Negri, F.; Castiglioni, C.; Tommasini, M.; Zerbi, G. A Computational Study of the Raman Spectra of Large Polycyclic Aromatic Hydrocarbons: Toward Molecularly Defined Subunits of Graphite. *J. Phys. Chem. A* **2002**, *106*, 3306–3317.
- (48) Frackowiak, E.; Gautier, S.; Gaucher, H.; Bonnamy, S.; Beguin, F. Electrochemical Storage of Lithium in Multiwalled Carbon Nanotubes. *Carbon* **1999**, *37*, 61–69.
- (49) Zhang, S.; Liu, H.; Huang, C.; Cui, G.; Li, Y. Bulk Graphdiyne Powder Applied for Highly Efficient Lithium Storage. *Chem. Commun.* **2015**, *51*, 1834–1837.
- (50) Lan, D. N.; Li, Q. Manipulating Local Chemistry of Phosphorus for High-Performance Sodium Ion Battery Anode Applications. *ACS Appl. Energy Mater.* **2019**, *2*, 661–667.
- (51) Pan, D.; Wang, S.; Zhao, B.; Wu, M.; Zhang, H.; Wang, Y.; Jiao, Z. Li Storage Properties of Disordered Graphene Nanosheets. *Chem. Mater.* **2009**, *21*, 3136–3142.
- (52) Yao, X.; Zhao, Y. Three-Dimensional Porous Graphene Networks and Hybrids for Lithium-Ion Batteries and Supercapacitors. *Chem.* **2017**, *2*, 171–200.
- (53) Lian, P.; Zhu, X.; Liang, S.; Li, Z.; Yang, W.; Wang, H. Large Reversible Capacity of High Quality Graphene Sheets as an Anode Material for Lithium-Ion Batteries. *Electrochim. Acta* **2010**, *55*, 3909—3914.
- (54) Xu, K. Electrolytes and Interphases in Li-Ion Batteries and Beyond. Chem. Rev. 2014, 114, 11503-11618.
- (55) Bratsch, S. G. Standard Electrode Potentials and Temperature Coefficients in Water at 298.15 K. J. Phys. Chem. Ref. Data 1989, 18, 1–21.
- (56) Cardona, C. M.; Li, W.; Kaifer, A. E.; Stockdale, D.; Bazan, G. C. Electrochemical Considerations for Determining Absolute Frontier Orbital Energy Levels of Conjugated Polymers for Solar Cell Applications. *Adv. Mater.* **2011**, 23, 2367–2371.
- (57) Frackowiak, E.; Béguin, F. Electrochemical Storage of Energy in Carbon Nanotubes and Nanostructured Carbons. *Carbon* **2002**, *40*, 1775–1787.
- (58) Sui, Z. Y.; Wang, C. Y.; Yang, Q. S.; Shu, K. W.; Liu, Y. W.; Han, B. H.; Wallace, G. G. A Highly Nitrogen-Doped Porous Graphene an Anode Material for Lithium Ion Batteries. *J. Mater. Chem. A* 2015, 3, 18229–18237.
- (59) Shu, K. W.; Wang, C. Y.; Wang, M.; Zhao, C.; Wallace, G. G. Graphene Cryogel Papers with Enhanced Mechanical Strength for High Performance Lithium Battery Anodes. *J. Mater. Chem. A* **2014**, 2, 1325–1331.
- (60) Schick, T. H. G.; Lauer, J. C.; Rominger, F.; Mastalerz, M. Transformation of Imine Cages into Hydrocarbon Cages. *Angew. Chem., Int. Ed.* **2019**, 58, 1768–1773.
- (61) Rice, A. M.; Dolgopolova, E. A.; Shustova, N. B. Fulleretic Materials: Buckyball- and Buckybowl-Based Crystalline Frameworks. *Chem. Mater.* **2017**, *29*, 7054–7061.
- (62) Rice, A. M.; Dolgopolova, E. A.; Yarbrough, B. J.; Leith, G. A.; Martin, C. R.; Stephenson, K. S.; Heugh, R. A.; Brandt, A. J.; Chen, D. A.; Karakalos, S. G.; Smith, M. D.; Hatzell, K. B.; Pellechia, P. J.; Garashchuk, S.; Shustova, N. B. *Angew. Chem., Int. Ed.* **2018**, *57*, 11310–11315.